A flat flame burner for the calibration of laser thermometry techniques

2006 Meas. Sci. Technol. 17 2485

(http://iopscience.iop.org/0957-0233/17/9/016)

INSTITUTE OF PHYSICS PUBLISHING MEASUREMENT SCIENCE AND TECHNOLOGY

Meas. Sci. Technol. **17** (2006) 2485–2493 doi:10.1088/0957-0233/17/9/016

A flat flame burner for the calibration of laser thermometry techniques

G Hartung, J Hult and C F Kaminski

Department of Chemical Engineering, University of Cambridge, Pembroke Street, Cambridge CB2 3RA, UK

E-mail: clemens_kaminski@cheng.cam.ac.uk

Received 2 May 2006, in final form 29 June 2006
Published 17 August 2006
Online at stacks.iop.org/MST/17/2485

Abstract

The design and experimental characterization of a burner is described, which has favourable characteristics for the accurate calibration of a range of optical thermometry techniques. The burner supports stable laminar flames and combines many of the advantages of several widely used burner designs without their disadvantages. It permits the application of point measurement techniques, line-of-sight techniques and planar imaging techniques; trace species, such as metal atoms, can be easily introduced into the flame. The implementation of the burner is described, followed by the presentation of data obtained from coherent anti-Stokes Raman scattering (CARS) measurements and numerical simulations. Spatially resolved measurements were performed over the entire flame profile at three different stoichiometries and factors causing systematic and random errors are described in detail. Measurement errors on mean temperatures were determined to be less than 1%. The shot-to-shot measurement precision was determined to be 3.5–4.0% (FWHM of temperature probability density function). The burner design together with the data presented in this paper can be used for the validation and calibration, respectively, of a variety of combustion thermometry techniques. Complete details of the burner design together with the obtained temperature data will be provided on the World Wide Web. Other researchers intending to validate and calibrate their own laser-based thermometry techniques will be able to cost-effectively reconstruct this burner and adopt the characterization presented here, thus being able to apply it without the need of their own basic validation. The authors are confident that a reconstructed burner, which is applied under the same conditions, will yield the same high level of accuracy and precision as that presented in this paper.

Keywords: thermometry, laminar flat flame burner, coherent anti-Stokes Raman scattering, Na-line reversal

(Some figures in this article are in colour only in the electronic version)

1. Introduction

A variety of laser diagnostic techniques have been developed, which allow the exploration of a wide range of combustion parameters, e.g. temperature, species concentrations (radicals, molecules, soot, etc) and flow fields. Such techniques are most usefully calibrated in well-characterized laminar flames, where temperature, concentration and flow patterns are stationary and can be predictably controlled. A calibration flame should ideally fulfil the following criteria: first, a flat flame front is desired to prevent temperature gradients along the direction of the laser beam, typically arranged at right angles to the flow direction. Secondly, if line-of-sight (e.g. absorption) techniques are to be calibrated, a clear

separation is required between the region from which temperature is to be deduced (central flow) and regions which are not of interest (e.g. co-flow flame or laboratory air). The temperature is required to be as constant as possible throughout the central flow region. Thirdly, several techniques require atomic tracer species to be seeded into the reactant gas mixture, e.g. indium for two-line atomic fluorescence (TLAF) [1, 2] or sodium for Na-line reversal [3], and clogging of flow homogenizers (e.g. sintered burner plates) must be prevented. Fourthly, it is desirable to be able to stabilize flames over a wide range of stoichiometries on the burner.

Over the last few decades several burner types have been developed in this context. Laminar flat flame burners feature a flameholder, which either consists of a flat porous frit or a flat plate with drilled holes to stabilize the flame. Snellemann and Smit [4] and Wakai [5] both introduced burners for the application of the sodium line reversal technique. The flameholder in both burners consists of a drilled plate. These burners are both capable of being seeded with atomic tracers and can operate with a burning co-flow at the same stoichiometry as the central flow. The relatively large hole diameter and hole-to-hole distance of Snellemann and Smit's burner (hole diameter ∼0.9 mm, distance between holes: ∼0.7 mm) results in cone shaped flames stabilized above each hole. These flames merge to produce a corrugated flame sheet above the burner plate, which is not truly flat. Wakai's burner is symmetric along the burner's central axis, but the seeded and unseeded regions upstream of the flame holder were not kept completely separated resulting in an unclear separation of atomic tracer species between central flow and co-flow.

Padley and Sudgen [6] introduced a Meker-type burner where the central part of the flameholder consisted of a bundle of 100 tubes with an inner diameter of 0.055 mm resulting in an inner laminar flame of 1 cm diameter. This flame is surrounded by a shielding flame fed by the same mixture as the inner flame; the width of this surrounding ring is ∼1.5 mm. Additional shielding is provided by an outer flame with the same mixture; however, the flameholder of this part is recessed, with respect to the rest of the burner surface, and is not designed to result in a laminar flame.

A burner which is widely applied is the commercially available non-premixed 'Hencken burner' [7]. The square, honeycomb-structured (diameter ∼0.9 mm) and uncooled burner holder is divided into a central flow and a co-flow. Within the central burner plate, fuel and oxidant are injected into alternating honeycomb channels. The fuel and oxidizer rapidly mix downstream of the honeycomb, forming an array of blended diffusion-like flamelets which quickly mix into a uniform post-combustion gas flow. A non-burnable shroud flow is introduced through an annular passage, which surrounds the central burner core. The total flow through this shroud is adjusted to match the velocity of the flow from the central core, thereby eliminating shear instabilities between the burner gases and the surrounding atmosphere. Additionally, diffusion of O_2 from the surrounding air is inhibited. The fact that the burner plate is un-cooled might lead to an undesired gradual increase of the flame temperature with time.

Snelling *et al* [8, 9] designed a burner consisting of an inner flame surrounded by an outer flame. The inner flame was stabilized on a steel honeycomb. The flameholder for the outer flow consisted of a sintered-bronze burner plate for the co-flow. CARS measurements revealed a 18 K higher temperature in the centre of the central flow compared to the mean temperature of the central flow. As the diameter of the seeded central flow of the burner plate is small the radial change in temperature is not negligible. As shown later on, if the central flow and co-flow are separated below the flameholder, the temperature map above the burner shows a depression in temperature due to the gap between the inner and outer flame fronts. Thus, the diameter of the burner plate for the central flow has to be large enough to avoid the effects of such a region on the temperature field near the centre of the flame.

The commercially available McKenna burner [10] has been the most commonly applied calibration burner for laser diagnostic applications and is characterized by a flat flame. However, this burner is not suitable for techniques which require atomic tracer species to be seeded into the reactant gas mixture (e.g. indium for TLAF or sodium for Na-line reversal method). The burner plate of the McKenna burner consists of a sintered plate which can easily become contaminated by small salt crystals, which are carried into the flame by the reactant gas to provide atomic tracer species. To the author's best knowledge no such applications have been reported in the literature. The co-flow is designed to be used for uncombustable gases, because of the lack of cooling provisions in the co-flow part of the burner plate. There are, thus, temperature/concentration gradients towards the outer parts of the flame, which make the device non-ideal for application of line of sight techniques (e.g. absorption measurements).

To summarize, the need for a burner arises which combines the advantages of the McKenna burner (pronounced flat flame and division into central and co-flow regions with matched flow profiles) and earlier developed burners, e.g. the Hencken burner (possibility of atomic tracer species to be seeded). The burner described in this paper combines all the features discussed above. The aim of this paper is to provide a well-characterized high temperature source which other researchers in the field of laser-based thermometry can simply reconstruct and apply for their calibration and validation purposes without having to characterize the high temperature source themselves. The complete details of the burner design will be provided on the Internet, allowing a cost-effective reconstruction. The authors are confident that a copy of the burner which is applied under the same conditions, will result in the same high level of accuracy and precision as that presented here. The temperature data shown here will be posted on the World Wide Web.

The following section describes the design of the burner in detail, followed by a discussion of salient features in the context of the diagnostics to be applied. Experimental details follow with results from CARS and Na-line reversal temperature measurements. A discussion on the determined temperature fields is presented and finally, the experimental data are compared with modelling results.

2. Burner design

A schematic of the flat flame burner is illustrated in figure 1. All parts were fabricated from brass, except the cooling tube, which was made of copper. The burner plate (thickness 5 mm)

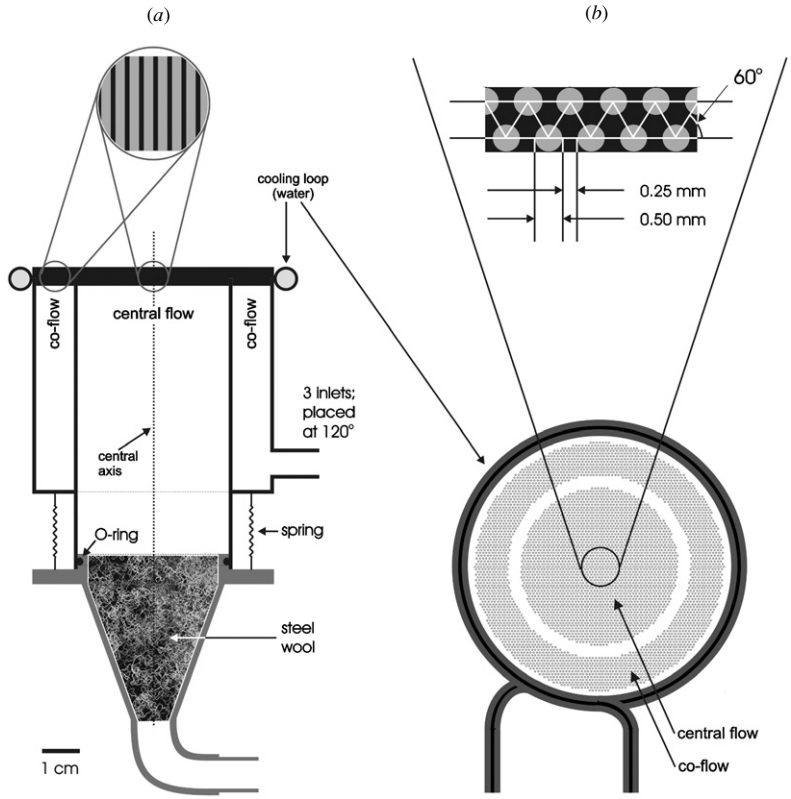

Figure 1. Calibration burner used to stabilize flat premixed methane/air flames. (*a*) Cross-section view, (*b*) top view.

consists of a brass disc with 2335 holes (diameter 0.5 mm) within the central part and 2696 holes (diameter 0.5 mm) for the co-flow. This design of the burner plate allows atomic seeding. As co-flow gas either N_2 or a premixed fuel and air mixture can be employed, the latter allows an 'outer flame' to be stabilized surrounding the inner flame, which is of particular interest for the application of line of sight techniques: using the same equivalence ratio for the inner and outer parts of the flame and, if required, seeding the inner part with an atomic tracer species, eliminates the effects of temperatures and concentration gradients at flame boundaries associated with unprotected flames. Heat transferred to the burner plate was effectively conducted away with a single water cooling loop (inner diameter 4 mm). The cooling loop was made of copper and was hard-soldered onto the circumference of the burner plate. The temperature of the burner plate did not rise by more than 10 °C, with respect to ambient temperatures, when using both the central and co-flow flames simultaneously (water temperature 15 °C, flow rate 1 l min^{-1}). As the diameters of the holes in the burner plate (0.5 mm) are much smaller than the minimum quenching diameter Φ_Q for a CH_4/air flame ($\Phi_Q = 2.5$ mm at 293 K [11] for quenching by a metal surface), flashback cannot occur. The burner is thus safe to use even with flames characterized by a Φ_Q significantly lower than the presently used flame, for example no flashback would occur on use of H_2/air flames [11].

The air and methane flows were regulated using rotameters (Solartron Mobrey Ltd) with needle control valves. The rotameter used for the airflow was a 3–30 l min^{-1} rotameter (2000-AH-14X-E-410), the one for the methane flow was a 1–6 l min^{-1} rotameter (1100-DE-H-F-300). The metering valve was located downstream of the flowmeter and the pressure in the meter maintained at 1.0 bar. The rotameters were calibrated to an accuracy of 0.5% and precision of 1%. The influence of the precision of the flow rates on the adiabatic temperature will be discussed in detail in section 4. To dampen pressure oscillations, the air flow was passed through two 25 litre vessels arranged in series, both of which were filled to one third with 1 cm diameter glass beads.

The design described results in very stable flames with one-dimensional temperature and concentration profiles along the flow direction, and allows for easy seeding of atomic tracer species. These characteristics allow the burner to be applied for all laser-based thermometry techniques and laser-based concentration measurements (major species, radical concentration and soot). These features and the well-defined boundary conditions render the system ideal for the application of one-dimensional numerical codes. The presented burner is suitable for point diagnostics, such as coherent anti-Stokes Raman scattering (CARS) [12], TLAF [2], OH-LIF [13], laser induced incandescence (LII) [14] as well as line-of-sight techniques, such as line-reversal methods [4] and absorption measurement techniques [15]. Reversal techniques require atomic tracers (commonly sodium) to be seeded into the reactant mixture. The use of an unseeded burning co-flow prevents systematic shifts of measured temperature to lower values because there is no associated drop in temperature in the transition region between seeded and unseeded parts

Figure 2. Photograph of the model flat burner operating on CH_4/air at the stoichiometric ratio. Central flow: Na-seeded, co-flow: unseeded.

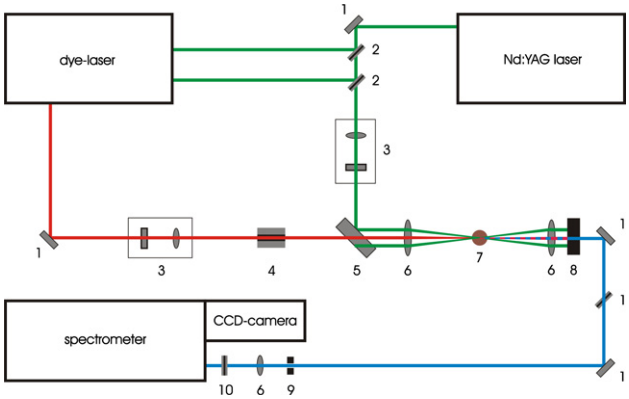

Figure 3. Optical set-up of CARS-temperature measurement experiment. (1) Dichroic mirror, (2) outcoupling mirror, (3) telescope, (4) cylindrical quartz block, (5) semicircular beamsplitter, (6) positive spherical lens, (7) burner, (8) beam dump, (9) slit, (10) Raman holographic edge filter.

of the flame. For line-of-sight absorption techniques (e.g. based on H_2O or CO_2 absorption [16]) an inert gas can be used as a co-flow which exactly defines the measurement volume. Thirdly, 2D-imaging techniques, such as OH-planar laser induced fluorescence (OH-PLIF) [17], NO-PLIF [18], LII [14], TLAF [2] are applicable.

Applying the Na-line reversal method in the burner described in this paper, with a Na-seeded central flow, a 20 K lower temperature was measured if the unseeded co-flow was omitted. In this case, air can be entrained into the boundary region between the hot burnt gases and the surrounding air, thus reducing the temperature at the flame edge. A hot unseeded co-flow with the same temperature as the central flow eliminates these systematically lower temperature readings. Figure 2 shows a photograph of the natural flame emission when the central flow is seeded with sodium and the co-flow remains unseeded. The picture shows that the entrainment of sodium into the co-flow is very small.

3. Experimental set-up

Temperature measurements were performed with the CARS [12, 19, 20] and Na-line reversal techniques [3, 4]. Vibrational CARS of N_2 was chosen because it is a well-established, non-intrusive method and its applicability for flame measurements has been proven in many applications.

The layout of the CARS set-up is shown in figure 3. A frequency-doubled Nd:YAG laser (Continuum Surelite II-10) operating at 10 Hz is employed as a pump source. The broadband Stokes radiation is generated by a dye laser (oscillator and a single amplifier). Both the oscillator and amplifier sections use a common dye cell positioned at the Brewster angle, which is longitudinally pumped. The total output of the dye laser is 7.5 mJ/pulse centred at 606 nm. To stabilize the dye spectral profile a bandpass filter was inserted into the dye cavity (dye laser output power: 7.5 mJ/pulse; dye laser spectral width: 6 nm FWHM). Galilean telescopes were incorporated into the pump and Stokes beams to control the beam diameter and focal spot location. To generate the CARS beam a folded BOXCARS phase matching geometry is used with a lens focal length of 300 mm and a pump laser energy of 60 mJ/pulse for each of the two green beams. The BOXCARS [12] half-angle employed was 0.9°. After passing a dichroic mirror to reflect residual 532 light and a Raman holographic edge filter the CARS signal beam was focused into a spectrometer (Spex, 2400 grooves mm^{-1}, $f =$ 1250 mm). The dispersed CARS spectra were recorded on a thinned chip, back illuminated CCD camera (384 × 576 pixels, Wright Instruments) with Peltier cooling and 14 bit dynamic resolution. Spectra were acquired at 10 Hz and 600 single shot spectra acquired for each measurement datum presented. To compensate for dye laser spectral profile variations and irregularities in the detection system, a non-resonant signal was recorded in propane. Dark signals (all beams blocked) were also acquired for both N_2 and propane spectra. Both non-resonant signal and dark signal were acquired at every 15th measurement point. The compensated CARS spectrum was obtained by dividing each background corrected resonant N_2 spectrum with the corresponding background corrected propane spectrum. The *CARSFIT* program [21], developed at Sandia National Laboratories, was used to fit the data to determine temperature.

The Na-line reversal method is an established non-intrusive optical technique for measuring flame temperatures. Na-atoms, seeded at trace levels into a flame, emit light at the two D-lines at 588.9950 nm and 589.5924 nm. In the line reversal method absorption of light from an incandescent calibrated tungsten lamp, which is applied as a temperature standard, by the sodium in the ground state and emission from the excited states of sodium are balanced by adjusting the temperature of the lamp. The sodium line will appear either as a bright line, standing out brighter than the blackbody continuum or in absorption, as a dark line against the continuum according to whether the brightness temperature of the blackbody source is lower or higher than the flame temperature. The 'reversal point' is attained when emission and absorption exactly balance, and the Na-lines thus disappear. The radiance temperature of the incandescent light source has to be variable over a range covering all temperatures to be measured. This method is only applicable in stable laminar flames, in which there is no temperature gradient along the Na-seeded part of the optical path. The flame was seeded by passing a portion of the air-fuel stream through a nebulizer containing an aqueous solution of NaCl (∼0.05 M), which

Table 1. Estimated uncertainties for rotameters (one scale division of 1 mm corresponds to a flow rate of 0.24 l min^{-1} for air and 0.022 l min^{-1} for CH_4).

Fluctuation of float rotometer at constant pressure	CH_4 Air	±0.25 ±0.50	Scale division
Fluctuation of pressure in rotometer	CH_4 Air	±0.007 ±0.017	Bar

resulted in a concentration of sodium atoms in the flame of approximately 100 ppb. This low seeding concentration was not observed to cause any perturbation to the flame properties. Possible systematic errors have been explored by Alkemade *et al* [3] and all efforts to minimize those have been made. The high accuracy of the Na-line technique stems from the fact that it is a null method that shifts the calibration to the background source and that strong resonance lines can be used, as self-absorption does not introduce an error. A radiance temperature calibration of the tungsten lamp applied was carried out using a ratiometric pyrometer (Landmark FRP12) resulting in a precision of better than 1% at 2000 K. The optical set-up employed and calibration procedures for the Na-line reversal applied were carefully investigated [22] and were similar to the set-up used by Snellemann [4].

Stereoscopic particle imaging velocimetry (PIV) measurements were also carried out to characterize the velocity field (Davis, Lavision, Germany) of the burnt gases above the burner. A pulsed 2nd harmonic Nd:YAG (32 mJ/pulse) was used to create a light-sheet of 480 μm thickness (FWHM). Both cameras (1280 × 1024 pixels; double-frame mode, Sensicam, PCO imaging, Germany) were arranged at 90° and corrected according to the Scheimpflug criterion. Particles (SiO_2, = 1–5 μm, Aerosil R 812, Degussa, Germany) were seeded into the reactive mixture with a fluidized bed followed by a cyclone.

4. Results

4.1. Errors due to flow rate fluctuations

The temperature measurements were carried out using CH_4/air gas mixtures at three stoichiometries ($\Phi = 0.8$, 1.0 and 1.2). At each stoichiometry, flow rates were decreased until a flat flame front was obtained. Variations in the methane and air gas flow rates respectively, cause changes in stoichiometry and thus the flame temperature. Deviations result from reading errors of the rotameter float position, errors in pressure gauge readings and pressure changes over time. The associated estimated errors are shown in table 1. For the stoichiometries applied experiments confirmed that these errors can be assumed to be independent of the flow rate applied. From these errors the range of most likely stoichiometries can be determined and, consequently, the associated spread of temperature [23]. This determines the best obtainable temperature precision 'within an experiment' (see figure 4). However, the calibration of the flowmeters is subject to similar reading errors resulting in the slightly wider temperature interval shown in figure 4 'experiment + calibration'. It can be seen that even with a well calibrated and stable flow system there is an appreciable temperature error associated with flow rate irregularities and thus their consideration is essential in the characterization of

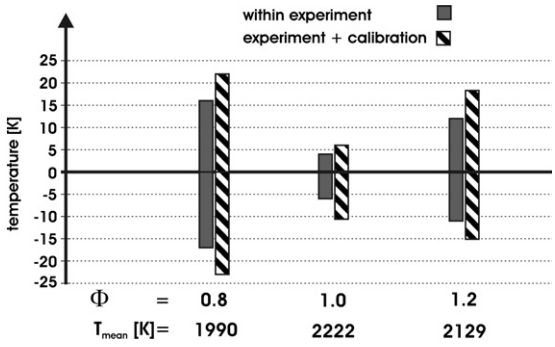

Figure 4. Resulting deviation in adiabatic temperature due to uncertainties in rotameter adjustment.

thermometry applications, but, surprisingly, is lacking in much of the previous literature. It is seen from figure 4 that the error is smallest around Φ=1 where the sensitivity of temperature to stoichiometry variations $dT/d\Phi$ is at a minimum. At $\Phi = 1.2$ the FWHM of the distribution is around 20 K, which may be appreciable compared to the precision of a high fidelity thermometry technique such as CARS.

4.2. Precision of CARS measurements

During CARS data collection the flow rates were carefully controlled to avoid any temporal drifts of the flame. For each set of acquired CARS-spectra (600 single shot spectra) the temporal trace of the obtained CARS-single shot-temperatures was investigated to explore for any instabilities. No significant systematic tendency over time could be observed.

The precision of the CARS-temperature measurements was established as follows: temperature measurements were performed near $\Phi = 1.0$ where flow and stoichiometry fluctuations have the least influence on temperature (see figure 4), with a temperature imprecision of only around 10 K. Early experiments exhibited that there were no vertical temperature gradients along the burner's central axis at a height of 12 mm above the burner plate (height above burner = HAB). The full-width-half-maximum (FWHM) obtained by a Gaussian fit to the single-shot temperature pdf (probability density function) typically showed a single-shot precision of 3.5–4.0% (FWHM/mean temperature), which is equivalent to a standard deviation of 1.8–2.0% (figure 5). This precision is similar to what has been reported using a single mode Nd:YAG laser in combination with a modeless dye laser [24], theoretically the optimal configuration for CARS as it minimizes noise due to coherent mode beating effects. Comparison of CARS experiments and Na-line reversal revealed an accuracy of the CARS-temperature measurements of better than 1.0% which is favourable compared to more expensive setups employing injection seeded pump and modeless dye laser systems. This is achieved through careful maximization of signal-to-noise ratios, by laser beam profile matching in the focal volumes, dye laser spectral profile optimization (see above). A crucial element of this precision is careful control of gas flow rates and removal of flow oscillations, which were found to be one of the most significant sources of potential errors. The day-to-day reproducibility of temperature measurements using both CARS and Na-line reversal techniques was better than the

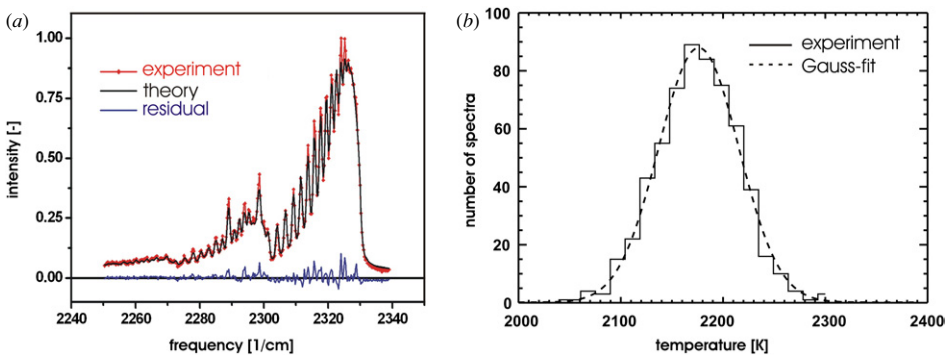

Figure 5. (*a*) Single shot CARS spectrum corresponding to a temperature of 2197 K, a theoretical fit is also shown as well as the residual; (*b*) temperature probability distribution functions evaluated from 600 single-shot vibrational CARS spectra taken in a CH_4/air flame at $\Phi = 1.0$.

measurement precision for both measurement techniques, and mean temperatures agreed to within 30 K at 2150 K from set-up to set-up. This adds confidence that adherence to the experimental protocols described here results in a highly reproducible and reliable temperature calibration system which is economical and easy to implement.

4.3. Temperature field

The temperature field distribution of the flame was mapped by setting up a grid of CARS-temperature measurements and piecewise cubic Hermite interpolation between the temperature points obtained. The measurement grid for the $\Phi = 1.0$ flame is shown in figure 6(*d*). At each measurement point 600 single shot spectra were acquired. The temperature of each single shot spectrum was obtained through a fit with CARSFIT and the most probable temperature obtained by a Gaussian fit to the pdf of the 600 evaluated temperatures (figure 5). Figures 6(*a*)–(*c*) show the fully mapped flame with interpolated data for the stoichiometries $\Phi = 0.8$, 1.0 and 1.2. The closest possible CARS-measurement location with respect to the burner plate was situated at HAB = 2 mm. This limitation is given by the BOXCARS arrangement employed (half-angle of 0.9°). It was thus not possible to fully resolve the temperature gradient across the flame front which was observed to be located at HAB between 0.8 and 1.1 mm. This will be discussed in more detail in the next section.

To decrease disturbances caused by air movements around the burner a cylindrical flow shield was used, which was attached to the burner. The chimney's inner diameter was 10 cm and it was placed 5 cm above the burner plate and its height was 22 cm. CARS measurements did not reveal any noticeable temperature difference at heights of 10, 20 and 30 mm with or without the presence of the shield. The measurement grids for $\Phi = 0.8$ and 1.2 are slightly different to that at $\Phi = 1.0$ to resolve regions, matched to the slightly different flame shape at these stoichiometries, in an effort to increase resolution near regions where temperature gradients were largest. Note the 'flattening' of the flame cone evident in figures 6(*a*)–(*c*) as one moves away from $\Phi = 1.0$ which is a manifestation of decreasing flame speeds. Each temperature map was constructed from approximately 45 000 to 50 000 single shot spectra.

All stoichiometries show a distinctive, well-resolved drop of temperature above the ring between the inner and the

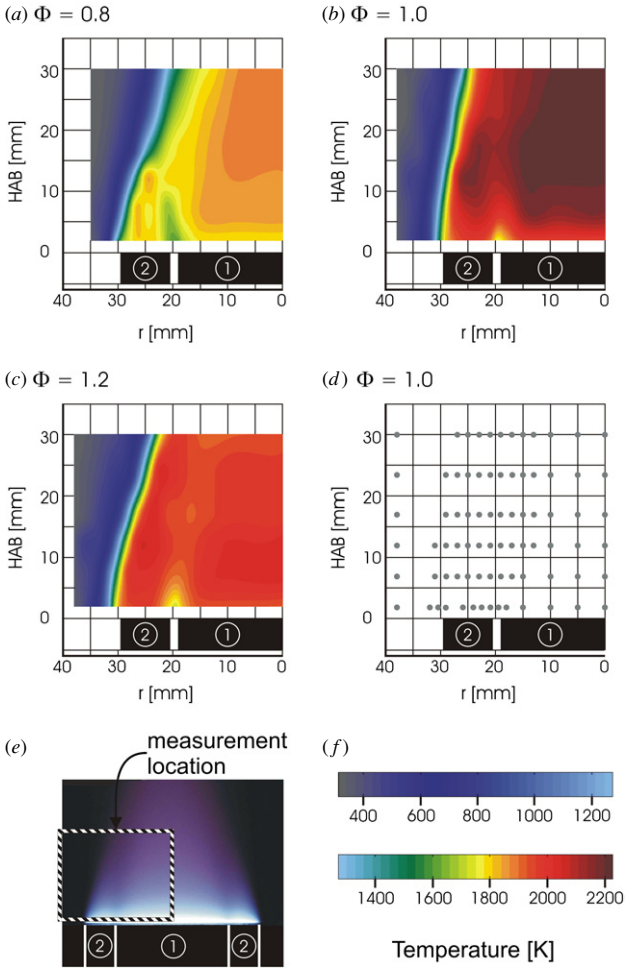

Figure 6. (*a*)–(*c*) 2D-temperature fields determined using CARS. Central and co-flow were operated at the same stoichiometry. (*d*) Measurement grid for $\Phi = 1.0$. (*e*) Photograph of flame with region of interest. (*f*) Temperature scale for figures (*a*), (*b*) and (*c*). ① = central flow; ② = co-flow.

outer flow, which is diminishing with HAB. The white bar between (1) and (2) in figures 6 and 7 depicts the hole-free region in the burner plate between central and co-flow. For all stoichiometries the lowest temperature measured at a height of 2 mm is 10–11% lower compared to the temperature

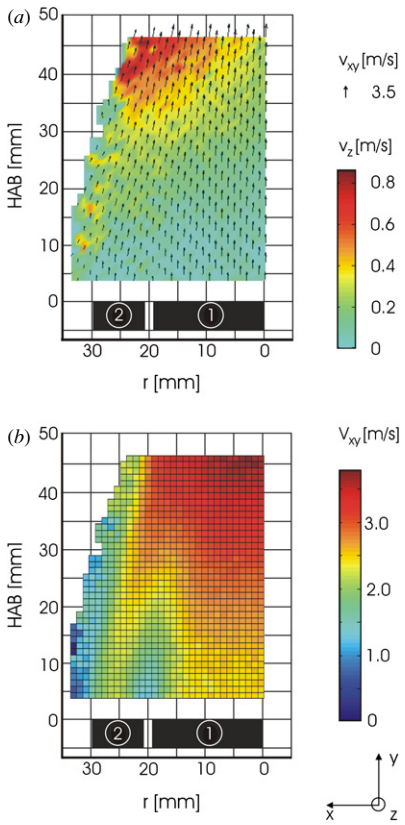

Figure 7. Velocity field of the burnt gases using stereoscopic PIV; central and co-flow were operated at the same stoichiometry ($\Phi = 1.0$); ① = central flow; ② = co-flow; (*a*) plot of v_{xy} and v_z, (*b*) plot of v_{xy} (x = radial position in the plane of the laser sheet, y = vertical position, z = radial position perpendicular to laser sheet).

at the same height at the burner plate's centre. For both stoichiometries of $\Phi = 0.8$ and $\Phi = 1.0$ the inner and outer flow patterns merge into one uniform structure whereas for $\Phi = 1.2$ the original flow structure seems to remain to some extent. The spatial location and extent of the regions of lower velocities of the *xy*-PIV velocity vector field shown in figure 7(*b*), carried out at $\Phi = 1.0$, is consistent with the location and extent of the homogeneous temperature region shown in figure 6(*b*). The depression of the temperatures and *xy*-velocities above the gap between the inner and outer flame fronts is clearly visible in both figures. This depression is thought to result from the merging of the originally separated central flow and co-flow to one homogenous flow. The reduced *xy*-flow velocities in the regions between inner and outer flame fronts near the burner plate result in longer residence times of the burnt gases which in turn lead to higher heat losses to the cooled burner plate. Increased heat loss to the burner plate explains why lower temperatures are observed in this region.

For all stoichiometries shown, the flames exhibit a highly homogenous post-combustion zone. For $\Phi = 1.0$ the temperatures in the post-combustion zone are homogeneous from 10 mm up to 30 mm above the burner and from the burner's axial centre $r = 0$ mm to $r \approx 12$ mm (figure 6(*b*)). This is underlined by the uniform direction of the *xy*-velocity vectors in this region (figure 7(*a*)). Figure 7(*a*) illustrates that the horizontal velocity component (v_z) is negligible in this region, which is of uttermost interest for calibrations and validations.

For $\Phi = 0.8$ it does take longer until a constant level of temperature is reached, which is at ~13 mm above the burner plate. Due to the lower flame speed and thus flow rate at $\Phi = 0.8$, the radial width of the homogeneous post-combustion zone is only 9 to 10 mm wide in contrast to ~12 mm at $\Phi = 1.0$. At $\Phi = 1.2$, however, a continuous decrease of temperature in the post-combustion zone is observed.

4.4. Theoretical flame calculations

A comparison of the temperature height profile in the calibration burner between CARS, Na-line reversal and model flame calculations was carried out for the three stoichiometries for which experimental data are presented: $\Phi = 0.8$, 1.0 and 1.2. The laminar premixed flame model calculations were conducted using the PREMIX code [25] for burner stabilized one-dimensional flames with a known mass flow rate. This code, developed at Sandia National Labs, uses data and subroutines from the CHEMKIN library to consider the detailed reaction mechanism, and uses transport packages to determine the accurate transport properties of the gas. Heat losses due to radiation are neglected in the model but are expected to be small for lean to stoichiometric flames. The experimental temperature height profiles were used as input for a first temperature guess to solve the energy equation. For these calculations, an air composition of 21% oxygen and 79% nitrogen was assumed and the unburnt gas temperature was set to 288 K.

The results of the comparison are shown in figure 8. For all stoichiometries the CARS measurements agree well with the calculated temperature profiles within the achievable measurement precision for heights greater than 7 mm. Experimentally, the flame front was observed to be at a height of 0.8–1.1 mm above the burner plate for all stoichiometries. The flame calculations in PREMIX resulted in a flame front between 0.35 and 0.45 mm above the burner plate, thus differing by 0.55 mm from the experimental flame front. If the flame front were used as a reference point to plot experimental and calculated temperature values for different HAB (by adding 0.55 mm to each HAB value of the PREMIX data), the calculated temperature value at 2 mm height would lie within the error margin of the CARS measurement. However, such a correction was not applied to the data in figure 8.

Depending on the stoichiometry, a steady state is obtained at different heights. The steady state might be defined to be obtained once CO_2- and OH-concentrations and temperature change only by approximately 0.25% and 5 K, respectively. Thus the exhaust gas is, in this approximation, practically in a steady state at HAB of ~7 mm for $\Phi = 0.8$, ~15 mm for $\Phi = 1.0$ and ~10 mm for $\Phi = 1.2$. For $\Phi = 1.2$, however, a gradual decrease of temperature is observed with increasing height.

The results of Na-line reversal measurements at HAB = 12 mm plotted in figure 8 are in good agreement with CARS measurements and model calculations. Those Na-line reversal measurements represent an independent validation method. Further details of the Na-line reversal validation measurements will be presented in a separate manuscript [22].

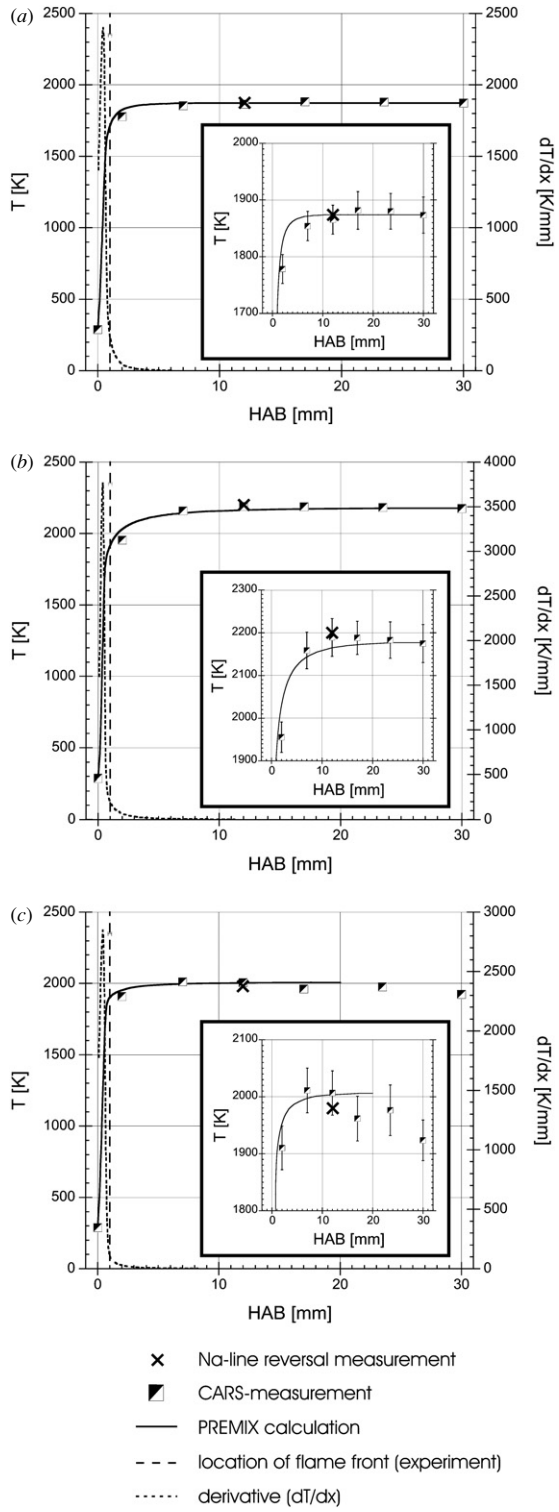

Figure 8. Comparison of temperature height profiles in the calibration burner measured using CARS and calculated using PREMIX for three stoichiometries: $\Phi = 0.8$, 1.0 and 1.2.

5. Summary and conclusion

A flat flame burner has been presented, which is suitable for calibration and validation purposes of a multitude of laser diagnostic techniques. The main merits of the burner are as follows: first, it shows a pronounced flat flame; second, good spatial uniformity is provided ($\leqslant$15 K) along the burner's central axis in the post-combustion region; third, temperature and concentrations are stable over time; fourth, the burner is suitable for burnable gas mixtures with a higher adiabatic gas temperature than CH_4/air due to high heat removal rate from the burner plate; and fifth, good optical access is provided. The design of the burner and a experimental CARS database will be posted on the Web [26].

Coherent anti-Stokes Raman scattering, the Na-line reversal method and theoretical model calculations (PREMIX) were applied in combination with stereoscopic PIV to validate the characteristics of the flat flame burner presented in this paper. CARS measurements revealed the radial and vertical temperature gradients in the post-combustion zone to be small. CARS measurements supplied a single shot precision of 1.8–2.0% (standard deviation). A sensitivity and error analysis revealed that possible temperature fluctuations due to flow-rate fluctuations of the unburnt gases were less than $\pm$6 K for the stoichiometric flames used in the current set-up. The absolute temperature values obtained by means of CARS were found to be in good agreement with PREMIX model calculations.

A well-characterized high temperature source has been presented, which other researchers in the field of laser diagnostics can easily reconstruct and apply for their own calibration and validation purposes without the need of further characterization. The complete details of the burner design as well as the obtained temperature data will be provided on the Web [26]. This burner could be applied as an international standard burner of the International workshop of measurement and computation of turbulent non-premixed flames (TNF).

Acknowledgments

This work was supported by grants from the EPSRC and grants from Rolls Royce within INTELLECT DM (Integrated lean low emission Combustor design methodology; FP6–502961). GH is grateful to a case studentship from CMI (Cambridge-MIT Institute). JH was supported by an Advanced Research Fellowship from the EPSRC. CFK thanks the EPSRC for the provision of a PLATFORM grant and the Leverhulme trust for personal sponsorship.

References

[1] Burns I S, Hult J, Hartung G and Kaminski C F 2006 A thermometry technique based on atomic lineshapes using diode laser LIF in flames *Proc. Combustion Institute* at press

[2] Hult J, Burns I S and Kaminski C F 2005 Two-line atomic fluorescence flame thermometry using diode lasers *Proc. Combustion Institute* vol 30 pp 1535–43

[3] Alkemade C T J, Hollander T, Snellemann W and Zeegers P J Th 1982 *Metal Vapours in Flames* (*International Series in Natural Philosophy* vol 103) (Oxford: Pergamon)

[4] Snelleman W and Smit J A 1968 A flame as a secondary standard of temperature *Metrologia* **4** 123–34

[5] Wakai K http://www.gifu-u.ac.jp/~wakailab/research/Beginner/Burner/burner_e.html

[6] Padley P J and Sudgen T M 1958 Photometric investigations of alkali metals in hydrogen flame gases: IV. Thermal and

chemiluminescent effects produced by free radicals *Proc. R. Soc. Lond.* **248** 248–65
[7] Kulatilaka W D, Lucht R P, Hanna S F and Katta V R 2004 Two-color, two-photon laser-induced polarization spectroscopy (LIPS) measurements of atomic hydrogen in near-adiabatic, atmospheric pressure hydrogen/air flames *Combust. Flame* **137** 523–37
[8] Snelling D R, Smallwood G J and Parameswaran T 1989 Effect of detector nonlinearity and image persistence on cars derived temperatures *Appl. Opt.* **28** 3233–41
[9] Snelling D R, Smallwood G J, Sawchuk R A and Parameswaran T 1987 Precision of multiplex CARS temperatures using both single-mode and multimode pump lasers *Appl. Opt.* **26** 99–110
[10] Prucker S, Meier W and Stricker W 1994 A flat flame burner as calibration source for combustion research—temperatures and species concentrations of premixed H_2/air flames *Rev. Sci. Instrum.* **65** 2908–11
[11] Griffiths J F and Barnard J A 1995 *Flame and Combustion* 3rd edn (Glasgow: Blackie)
[12] Eckbreth A C 1988 *Laser Diagnostics for Combustion Temperature and Species* (Kent: Abacus)
[13] Kohse-Höinghaus K and Jeffries J B 2002 *Applied Combustion Diagnostics (Combustion: An International Series)* (New York: Taylor and Francis)
[14] Moreau C S, Therssen E, Mercier X, Pauwels J F and Desgroux P 2004 Two-color laser-induced incandescence and cavity ring-down spectroscopy for sensitive and quantitative imaging of soot and PAHs in flames *Appl. Phys.* B **78** 485–92
[15] Webber M E, Kim S, Sanders S T, Baer D S, Hanson R K and Ikeda Y 2001 *In situ* combustion measurements of CO_2 by use of a distributed-feedback diode-laser sensor near 2.0 m *Appl. Opt.* **40** 821–8
[16] Allen M G 1998 Diode laser absorption sensors for gas-dynamic and combustion flows *Meas. Sci. Technol.* **9** 545–62
[17] Balachandran R, Ayoola B O, Kaminski C F, Dowling A P and Mastorakos E 2005 Experimental investigation of the nonlinear response of turbulent premixed flames to imposed inlet velocity oscillations *Combust. Flame* **143** 37–55
[18] Nygren J, Engstrom J, Walewski J, Kaminski C F and Aldén M 2001 Applications and evaluation of two-line atomic LIF thermometry in sooting combustion environments *Meas. Sci. Technol.* **12** 1294–303
[19] Attal-Tretout B, Bouchardy P, Magre P, Pealat M and Taran J P 1990 CARS in combustion—prospects and problems *Appl. Phys.* B **51** 17–24
[20] Schneider-Kühnle Y 2005 Experimentelle Untersuchung rußender Hochdruckflammen mit laserdiagnostischen Messmethoden *Forschungsbericht 2005–06* (Köln: Deutsches Zentrum für Luft- und Raumfahrt)
[21] Palmer R E 1989 The CARSFT computer code for calculating coherent anti-Stokes Raman spectra: user and programmer information *Sandia National Laboratories Report* SAND89-8206, Livermore, CA
[22] Hartung G, Walewski J W, Hult J F and Kaminski C F 2005 Brightness–temperature calibration of a tungsten incandescence lamp; Part I: experimental considerations and systematic error sources; Part II: thorough statistical analysis unpublished data
[23] Morley C 2004 Gaseq—chemical equilibrium in perfect gases (Version 0.79) http://www.gasequationco.uk
[24] Kuehner J P, Woodmansee M A, Lucht R P and Dutton J C 2003 High-resolution broadband N_2 coherent anti-Stokes Raman spectroscopy: comparison of measurements for conventional and modeless broadband dye lasers *Appl. Opt.* **42** 6757–67
[25] Kee R J, Grcar J F, Smooke M D and Miller J A 1993 A FORTRAN program for modelling steady laminar one-dimensional premixed flames *Sandia National Laboratories Report* SAND85-8240
[26] http://www.cheng.cam.ac.uk/research/groups/laser